EFFECT OF CARBON NANOTUBE LOADING ON THE CORROSION BEHAVIOR AND HARDNESS OF Ni-P-CARBON NANOTUBE COMPOSITE COATINGS OBTAINED BY AUTOCATALYTIC DEPOSITION ON API 5L X80 PIPELINE STEEL

Mara Cristina Lopes de Oliveira, mara.oliveira@usp.br[1]
Laís Bezerra Bertunes, lais.bertunes@hotmail.com [2]
Renato Altobelli Antunes, renato.antunes@ufabc.edu.br[2]
Olandir Vercino Correa, ovcorrea@ipen.br[3]

[1]Electrocell Ind. Com. De Equip. Elétricos LTDA, CIETEC, Av. Prof. Lineu Prestes, 2242, São Paulo – SP, 05508-900
[2]Universidade Federal do ABC (UFABC), Centro de Engenharia, Modelagem e Ciências Sociais Aplicadas (CECS), Av. Dos Estados, 5001, Santo André – SP, 09210-580
[3]Instituto de Pesquisas Energéticas e Nucleares (IPEN/CNEN-SP), Centro de Ciência e Tecnologia de Materiais (CCTM), Av. Prof. Lineu Prestes, 2242, Cidade Universitária, São Paulo – SP, 05508-000

Abstract. *The aim of the present work was to incorporate multiwalled carbon nanotubes (MWCNTs) into Ni-P coatings obtained by electroless deposition on API 5L X80. Additionally, the effect of MWCNT concentration on the corrosion resistance of the deposited films was investigated. Film morphology was evaluated by scanning electron microscopy. Differential scanning calorimetry and x-ray diffraction were used to characterize the film structure. The electrochemical behavior of the composite layers was evaluated by electrochemical impedance spectroscopy and potentiodynamic polarization. The films presented crystalline nature but tend to become more amorphous as the carbon nanotube concentration in the bath increased. The presence of MWCNTs did not influence the DSC curves with respect to conventional Ni-P coatings. Film morphology was influenced by the MWCNTs, showing a decrease of metal nodules as the nanometric filler concentration increased. As a result, the corrosion behavior was affected as well. For higher filler loadings, the corrosion resistance increased due to the more compact surface morphology.*

Keywords: Ni-P-carbon nanotube coating, electroless deposition, corrosion, API 5L X80 pipeline steel

1. INTRODUCTION

Carbon nanotubes (CNTs) are attractive materials due to an impressive combination of properties such as high thermal and electrical conductivities and excellent mechanical strength (Cubides and Castaneda, 2016). Incorporation of CNTs in metallic coatings has been reported as a viable alternative of enhancing wear and corrosion properties of engineering components (Chen et al., 2005). Lee et al. (2012) evaluated the wear and corrosion properties of electrodeposited Ni-CNT coatings on Ti-6Al-4V alloy substrates. They observed that CNTs addition led to hardness increase to the combined effect of particle dispersion strengthening mechanism and the intrinsic high hardness of CNTs. This effect was accompanied by coefficient of friction reduction that was ascribed to the lubricating character of CNTs. Moreover, the improved resistance against corrosion was due to the compactness of the protective coating. Other authors have highlighted the beneficial effect of CNTs as a corrosion mitigating agent due to its intrinsic low chemical reactivity (Hammer et al., 2013).

The outstanding set of attributes described in the previous paragraph has driven the development Ni-P-CNT composite coatings produced by electroless deposition. Conventional electroless deposited Ni-P coatings are well-established protective films against wear and corrosion of metallic parts in different industrial applications, being suitable to cover uniformly even parts with complex geometry (Liu et al., 2016; Luo et al., 2015). CNT incorporation into the standard Ni-P layers can give rise to improved properties with respect to degradation resistance against wear and corrosion, thus expanding its applications to increasingly harsh environments (Chen et al., 2003). The protection of pipeline steels used for transportation of oil and gas in the petrochemical industry is one example of industrial usage for Ni-P-CNT coatings. In order to prevent these components from internal corrosion a series of different surface coatings have been proposed. Electroless deposited Ni-P-based films play a central role in this scenario (Mirza et al., 2016).

In spite of the favorable technological characteristics and the successful development of Ni-P-CNT coatings produced by electroless deposition, some challenges are still remaining for obtaining optimum performance against wear and corrosion. The aim of the present work was to study the effect of multi-walled carbon nanotube concentration on the corrosion resistance and surface morphology of Ni-P-CNT coatings produced by electroless deposition. Film structure was studied by differential scanning calorimetry (DSC) and X-ray diffraction.

2. MATERIALS AND METHODS

2.1 Electroless deposition

The API 5L X80 pipeline steel plate used as substrate for the electroless deposition of Ni-P-CNT coatings was kindly provided by Usiminas (Brazil). Its chemical composition is shown in Tab. 1. The specimens for deposition were cut from the originally provided plate in rectangular pieces with 20 mm x 30 mm x 5 mm. These pieces were ground using SiC paper up to grit 1200, being subsequently cleaned by washing with deionized water and dry in a warm air stream.

Table 1. Chemical composition of the API 5L X80 pipeline steel used in the present work.

Massa	C	Mn	Si	P	S	Nb	Al	Cr	V	Fe
(%)	0.04	1.75	0.20	0.02	0.002	0.065	0.025	0.11	0.025	Bal.

The base composition of the plating bath is shown in Tab. 2. All chemicals were pure analytical grade reagents. Multi-walled carbon nanotubes were purchased from UFMG (Brazil) and were used without any previous treatment. Three different concentrations of CNTs were added to the plating bath: 0.25 $g.L^{-1}$, 0.50 $g.L^{-1}$ and 1.0 $g.L^{-1}$. The Ni-P-CNT coatings are designated as CNT1, CNT2 and CNT3, respectively. Before deposition the specimens were cleaned in an alkaline solution consisting of 10 wt.% NaOH at 50 °C and activated in a 50 %vol. H_2SO_4 solution at room temperature. After washing with deionized water, the specimens were immersed in the plating bath. Total deposition time was 2 h. After deposition, the specimens were annealed at 400 °C for 1 h in a tubular furnace under argon atmosphere, followed by cooling inside the furnace. This is a common procedure to promote the formation of hard nickel phosphides that increase hardness of Ni-P coatings obtained by electroless deposition (Hu et al., 2006).

Table 2. Composition of the plating bath and operating conditions.

$NiSO_4.6H_2O$	
$Na_2H_2PO_2.H_2O$	
$Na_3C_6H_5O_7.2H_2O$	
CH_3COOH	
$C_3H_6O_3$	
NaOH	
Operating conditions	
pH	9.0
Temperature	88 ºC
Magnetic stirring	

2.2 Film characterization

The surface morphology of the deposited layers was examined with a scanning electron microscope (Hitachi TM3000). The crystallization behavior was assessed by differential scanning calorimetry (DSC) using a Shimadzu DSC60 instrument. The specimens were heated at 10 $°C.min^{-1}$ from the room temperature up to 500 °C under nitrogen atmosphere (flow rate of 30 $mL.min^{-1}$). The specimens for the DSC analyses were in the as-deposited state (not subjected to annealing). Coating crystalline structure was studied by X-ray diffraction (Rigaku DMAX-2000) using Cu-kα radiation. The specimens were scanned from 10° to 70° at a rate of $0.02°.min^{-1}$.

Nanoindentation tests were performed for the Ni-P and Ni-P-CNT coatings. The tests were performed using a NHT^2 Nanoindentation tester (Anton Paar) with a Berkovich indenter. Nanoindentation was carriet out at a loading rate of 100 mN/min, peak load of 50 mN and unloading rate of 100 mN/min. The peak load was applied for 2 s. The values of hardness and Young's modulus were determined from load versus penetration depth curves using the Oliver & Pharr method. The results reported here express the average of eight indentations per specimen.

Specimens for electrochemical characterization were prepared by connecting a copper wire at the back of the coated material. The electrolyte consisted of a 3.5 wt.% NaCl solution at room temperature. The experimental set-up was comprised of a conventional three-electrode cell arrangement, using a platinum wire as the counter-electrode, Ag/AgCl as reference and the Ni-P-CNT coated specimens as working electrodes. The open circuit potential (OCP) was monitored for 1 h to ensure a steady state condition. Electrochemical impedance spectroscopy (EIS) measurements were, then, carried out at the OCP in the range from 100 kHz to 10 mHz. The amplitude of the sinusoidal perturbation was 10 mV (rms) at an acquisition rate of 10 points per decade. Next, potentiodynamic polarization curves were

obtained from 300 mV versus the OCP up to 1.0 VAg/AgCl at a scanning rate of 1 $mV.s^{-1}$. The tests were performed in triplicate. The tests were performed using a potentiostat/galvanostat Autolab 101M.

3 RESULTS AND DISCUSSION

3.1 Film morphology and structure

Figure 1 shows SEM micrographs of the Ni-P and Ni-P-CNT coatings. The conventional Ni-P coating presented several nodules. The Ni-P-CNT coatings are more compact. In spite of the presence of some nodules, nodular structure is less marked for the CNT-containing layers. It is also noteworthy that the presence of the CNTs led to formation of some defects on the film surface. Notwithstanding, the morphology is more compact for the Ni-P-CNT films. The regions containing CNT particles increased with the CNT concentration in the plating bath, as indicated the more frequent small and dark features in Figs. 1c and 1d.

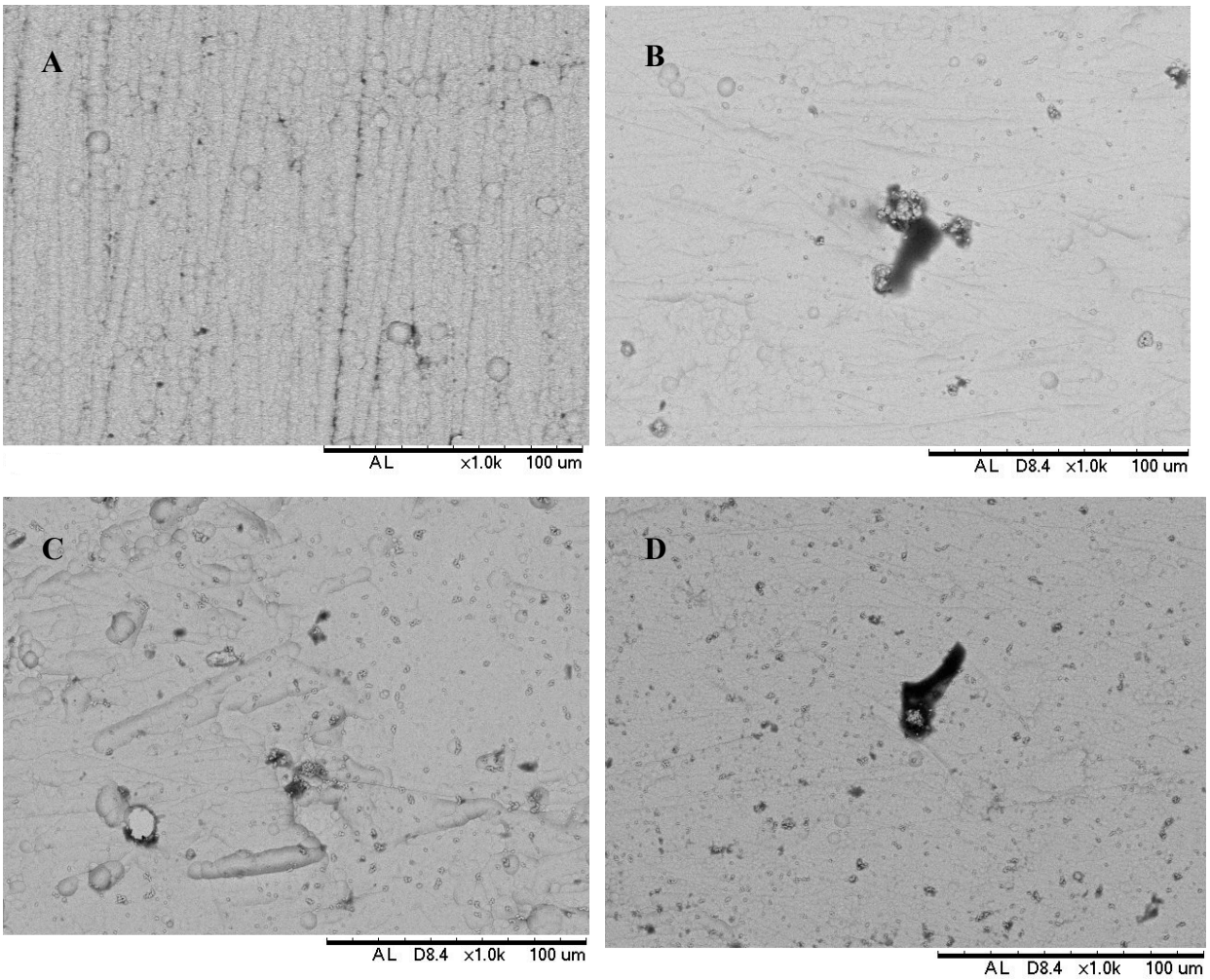

Figure 1. SEM micrographs of the Ni-P and Ni-P-CNT coatings after annealing at 400 °C for 1 h: a) Ni-P; b) CNT1; c) CNT2; d) CNT3.

DSC curves of the Ni-P and Ni-P-CNT coatings are shown in Fig. 2. The thermograms are characterized by the presence of exothermic peaks, irrespective of the CNT concentration in the plating bath, indicating that the as-deposited specimens crystallize during heating. The position of the crystallization peak is little affected by CNT concentration. Crystallization took place at approximately 347 ºC for all coatings. Exothermic peaks are associated with the precipitation of crystalline phases such as Ni_3P (Park and Lee, 1988). The main difference can be perceived for the DSC curve of the conventional Ni-P film which is characterized by the presence of two overlapping exothermic peaks. According to Palaniappa and Seshadri (2007) the second peak is often due to the transformation of a metastable phase into a stable crystalline phase.

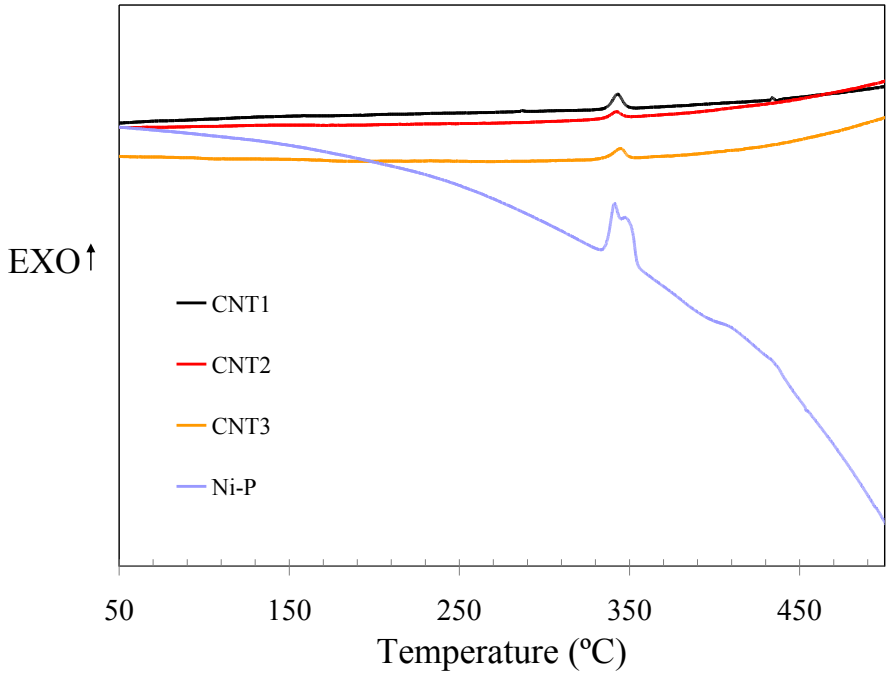

Figure 2. DSC curves of the Ni-P and Ni-P-CNT coatings.

X-ray diffraction patterns of the Ni-P and Ni-P-CNT coatings are shown in Fig. 3.

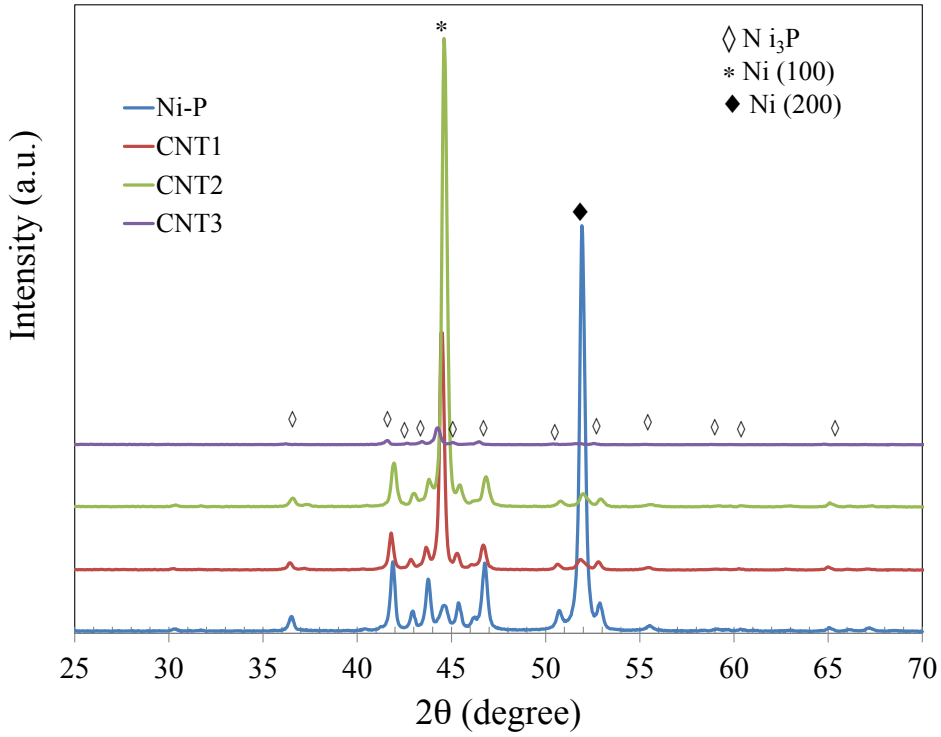

Figure 3. X-ray diffraction patterns of the Ni-P and Ni-P-CNT coatings.

The two main peaks at 44.5° and 51.8° correspond to reflections of Ni (111) and Ni (200) planes. Nickel nanometric crystallites are found on Ni-P coatings after annealing (Szczygiel et al., 2008). The crystalline state of the annealed coatings is confirmed by the presence of several reflections ascribed to Ni_3P phase. Phase transformations studies of electroless nickel deposits point to the precipitation of Ni_3P crystallites at temperatures above 350°C up to 500°C, depending on the composition of the plating bath (Liu et al, 2010). Diffractograms in Fig. 3 unequivocally confirm the presence of Ni_3P crystallites, independently of the carbon nanotube concentration in the plating bath. However, the crystalline character is greatly decreased for the CNT3 film. The reflections for the Ni and Ni3P phases are much less intense than for the other films, indicating that the incorporation of high carbon nanotube loadings makes the Ni-P coating more amorphous..

3.2 Corrosion tests

3.2.1 EIS measurements

Nyquist plots of the uncoated substrate and Ni-P-CNT coatings obtained after 1 h of immersion in 3.5 wt.% NaCl solution at room temperature are shown in Fig. 4. The inset shows the expanded scale plots in order to more clearly resolve the high frequency region of the EIS diagrams. This allows one to distinguish between the low-impedance uncoated substrate and the Ni-P-CNT coatings. The coated API 5L X80 steel presented a remarkable impedance increment with respect to the bare condition, indicating the coating barrier effect.

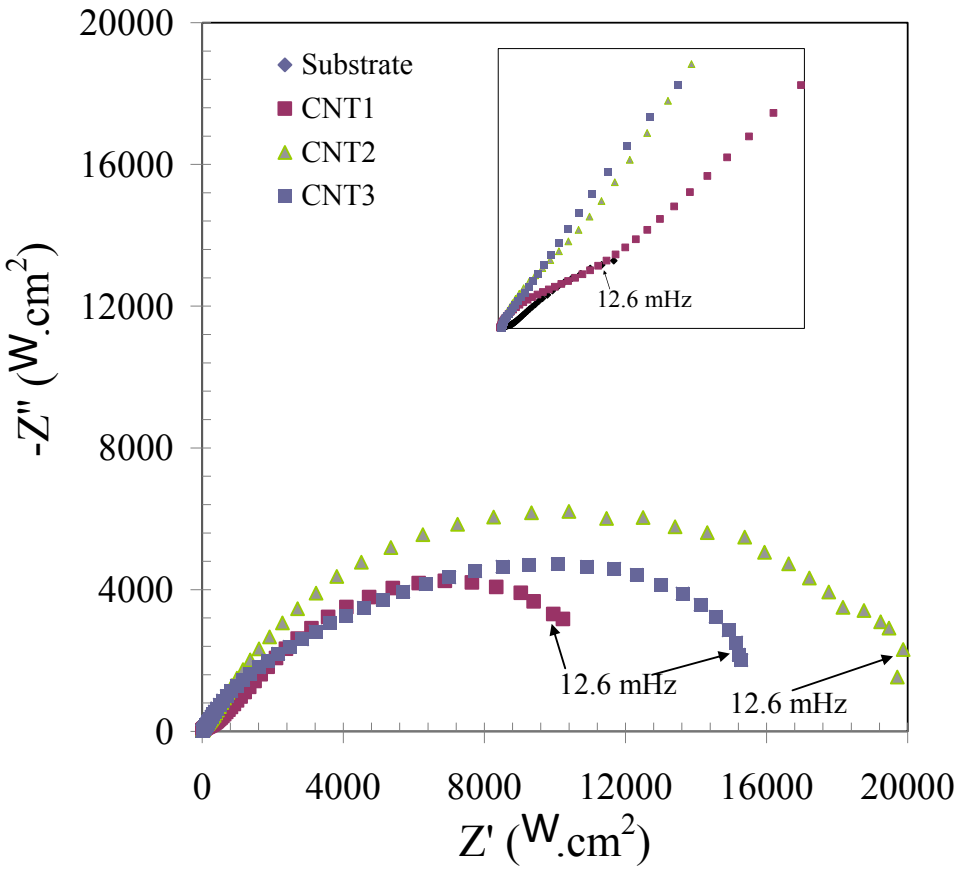

Figure 4. Nyquist plots of the uncoated substrate and Ni-P-CNT coatings after 1 h of immersion in 3.5 wt.% NaCl solution at room temperature.

The Nyquist plots are characterized by one flattened capacitive loop whose diameter is dependent on the CNT concentration on the plating bath. The diameter of the semicircle is related to the corrosion resistance of the electrode surface (Rabizadeh et al., 2010). The highest size of CNT2 semicircle suggests its corrosion resistance is superior to that of the other coatings. The lowest corrosion resistance would be accomplished by the CNT1 coating. The low chemical reactivity of CNTs is, therefore, an important factor to determine the corrosion properties of Ni-P-CNT coatings. If one considers film morphology, SEM micrographs suggest that increasing CNT loadings can lead to more surface defects on the coating. Nevertheless, this effect is apparently counterbalanced by the increased chemical stability imparted to the coating by the inert CNTs.

3.2.2 Potentiodynamic polarization

Potentiodynamic polarization curves of the uncoated substrate, Ni-P and Ni-P-CNT coatings were obtained right after the EIS measurements. The results are shown in Fig. 5. Corrosion parameters determined from polarization curves are displayed in Tab. 3.Values of corrosion potential (E_{corr}) and corrosion current density (i_{corr}) were determined using the Tafel extrapolation method, considering only the cathodic branches of the polarization curves.

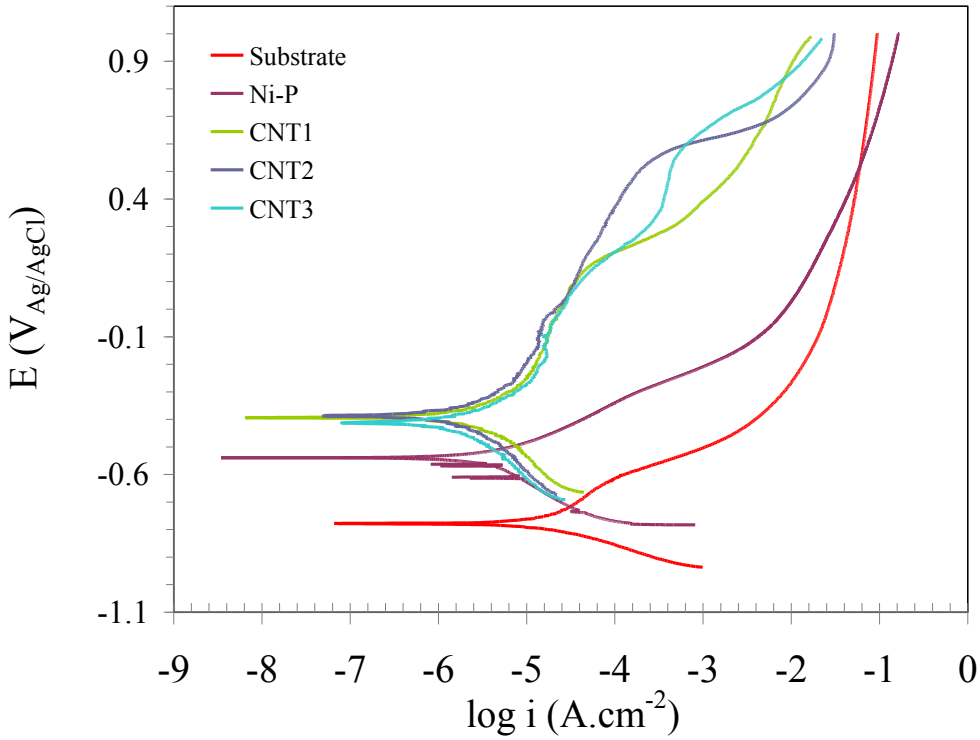

Figure 5. Potentiodynamic polarization curves of the uncoated substrate, Ni-P and Ni-P-CNT coatings.

Table 3. Corrosion parameters of the uncoated substrate, Ni-P and Ni-P-CNT coatings.

Coating	E_{corr} ($mV_{Ag/AgCl}$)	i_{corr} ($\mu A.cm^{-2}$)
Uncoated	-778	20.3
Ni-P	-540	4.17
CNT1	-394	3.28
CNT2	-388	2.38
CNT3	-413	2.01

The polarization curves clearly reveal that the anodic current densities of the Ni-P-CNT coatings are lower than those of the uncoated API 50 X80 steel and Ni-P film, indicating that dissolution is slowed down by incorporating the low reactivity CNTs into the Ni-P layer. The presence of CNTs have also increased the stability of the passive region which is hardly perceived in the polarization curves of the bare substrate and Ni-P film but extends though hundreds of mV for the CNT-containing coatings. The passive region is denoted by a small increase of the current density with the applied potential. This can be promptly seen in the curves of the Ni-P-CNT coatings. It is also observed that it is wider for the CNT2 and CNT3 films, indicating the higher corrosion resistance of these coatings with respect to CNT1, thus confirming the EIS results.

The corrosion parameters shown in Tab. 3 indicate that E_{corr} is shifted to less nobler values for the Ni-P-CNT coatings whereas i_{corr} decreased. E_{corr} is an indication of the propensity of an electrode surface to suffer anodic corrosion processes, being related to its thermodynamic stability. Higher values of E_{corr} are, therefore, associated with better corrosion resistance. In the same regard, low values of i_{corr} indicate that surface dissolution is slow, being related to the electrode corrosion rate (Musa et al., 2009; Liu et al., 2015). The low i_{corr} values of the highest CNT-loaded films (CNT2 and CNT3) would, then, reflect the chemical inertness of CNTs which is in agreement with the EIS results. In the same regard, the shift of E_{corr} to nobler values for the Ni-P-CNT coatings is also an indication of the beneficial effect of the chemical stability of CNTs to the corrosion properties of the electrolessly deposited films.

3.3 Nanindentation tests

Figure 6 shows typical load versus penetration depth curves for the Ni-P and Ni-P-CNT coatings. Hardness (H), Young's modulus (E) and the H/E ratio were determined from these curves and the values are reported in Tab. 4. The H/E ratio is related to the surface wear resistance, being employed as an indirect indication of this property for thin films (Leyland and Matthews, 2000).

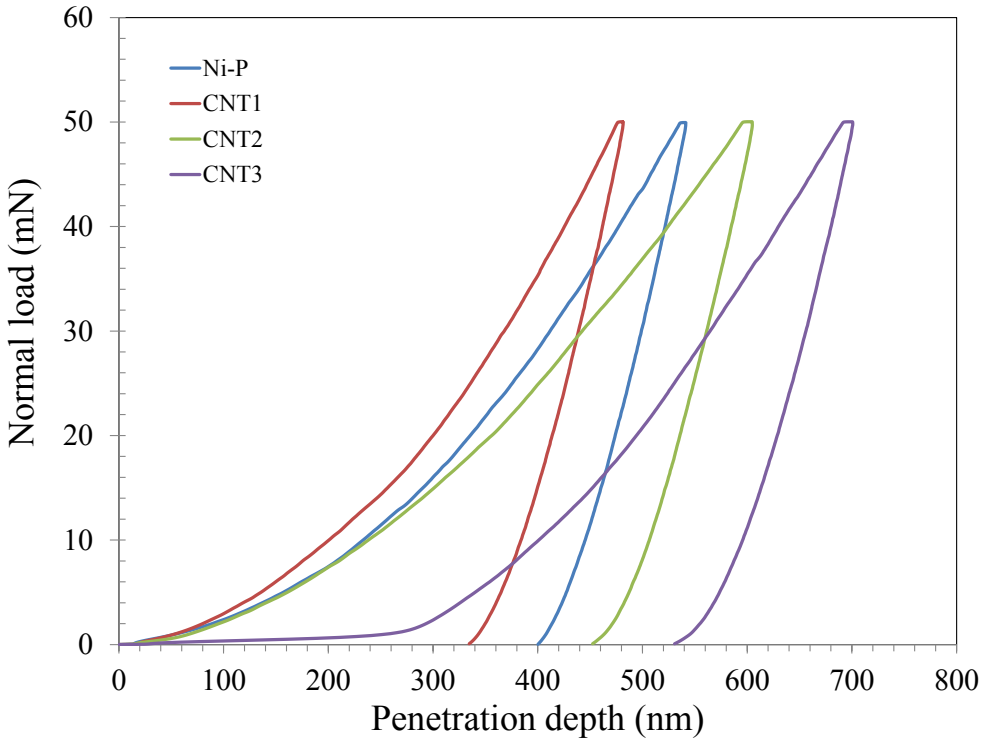

Figure 6. Load versus penetration depth curves for the Ni-P and Ni-P-CNT coatings.

Table 4. Hardness (H), Young's modulus (E) and H/E ratio for the Ni-P and Ni-P-CNT coatings.

Sample	H (MPa)	E (GPa)	H/E
Ni-P	10233	218	0.047
CNT1	13132	244	0.054
CNT2	7781	187	0.041
CNT3	5800	147	0.040

The results pointed that the only composite Ni-P-CNT coating with improved hardness with respect to the conventional Ni-P film was CNT1. Hardness and Young's modulus decreased as the carbon nanotube concentration in the plating bath increased. The curves in Fig. 6 point for a higher penetration depth as the CNT content increased. This effect was also perceived for the H/E ratio which decreased for CNT2 and CNT3 when compared with CNT1, indicating that the wear resistance decreases as the CNT loading is increased. The crystalline character of the composite layer is apparently related to the results obtained for the nanoindentation tests. According to Fig. 3, the Ni-P-CNT coating becomes more amorphous for higher CNT loadings. The hardness values shown in Tab. 4 indicate that the coating is softer when the film crystalline character is less marked.

3. CONCLUSIONS

Ni-P-carbon nanotubes composite coatings were successfully obtained by electroless deposition. Coating morphology was affected by carbon nanotube incorporation. Conventional Ni-P presents a nodular structure that becomes less marked with carbon nanotube addition. The crystallization temperature of the films was little affected by carbon nanotubes. The crystalline character, in turn, was dependent of the carbon nanotube concentration. The films become more amorphous for high carbon nanotube loadings. The corrosion resistance was higher for the more amorphous layers whereas hardness, in turn, was decreased.

4. ACKNOWLEDGEMENTS

The authors are thankful to Usiminas for kindly providing the API 5L X80 plate used in the present work and to CNPq (Process 470944/2013-7) for the financial support. Dr. Nelson Batista de Lima from IPEN/CNEN-SP is kindly acknowledged for the support with XRD analyses.

5. REFERENCES

Chen, C.H., Chen, C.S., Xiao, H.N., Cheng, F.Q., Zhang, G. and Yi, G.J., 2005, "Corrosion behavior of carbon nanotubes-Ni composite coating", Surface & Coatings Technology, vol. 191, pp. 351-356.

Chen, W.X., Tu, J.P., Xu, Z.D., Chen, W.L., Zhang, X.B. and Cheng, D.H., 2003, "Tribological properties of Ni-P-multi-walled carbon nanotubes electroless composite coating", Materials Letters, Vol. 57, pp. 1256-1260.

Cubides, Y. and Castaneda, H., 2016, "Corrosion protection mechanisms of carbon nanotube and zinc-rich epoxy primers on carbon steel in simulated concrete pore solutions in the presence of chloride ions", Corrosion Science, Vol. 109, pp. 145-161.

Hammer, P., dos Santos, F.C., Cerrutti, B.M., Pulcinelli, S.H. and Santilli, C.V., 2013, "Carbon nanotube-reinforced siloxane-PMMA hybrid coatings with high corrosion resistance", Progress in Organic Coatings, Vol. 76, pp. 601-608.

Hu, Y.-J., Wang, T.-X., Meng, J.-L. and Rao, Q.-Y., 2006, "Structure and phase transformation behavior of electroless Ni-W-P on aluminium alloy", Surface & Coatings Technology, Vol. 201, pp. 988-992.

Lee, C.K., 2012, "Wear and corrosion behavior of electrodeposited nickel-carbon nanotube composite coatings on Ti-6Al-4V alloy in Hanks' solution", Tribology International, Vol. 55, pp. 7-14.

Leyland, A. and Matthews, A., 2000, On the significance of the H/E ratio in wear control: a nanocomposite coating approach to optimized tribological behavior, Wear, Vol. 246, pp. 1-11.

Liu, H., Viejo, F., Guo, R.X., Glenday, S. and Liu, Z., 2010, Microstructure and corrosion performance of laser-annealed electroless Ni-W-P coatings, Surface & Coatings Technology, Vol. 204, pp. 1549-1555.

Liu, H., Lv, Y.Y., Liu, Z., Liu, H. and Thompson, G.F., 2016, "Dry sliding wear behavior and structural characteristics of laser-annealed electroless Ni-P/Ni-Mo-P duplex coatings", Tribology International, Vol. 103, pp. 343-351.

Liu, X., Xiang, Z., Niu, J., Xia, K., Yang, Y., Yan, B. and Lu, W., 2015, "The corrosion behaviors of amorphous, nanocrystalline and crystalline Ni-W alloys coating", International Journal of Electrochemical Science, Vol. 10, pp. 9042-9048.

Luo, H., Leitch, M., Behnamian, Y., Ma, Y., Zeng, H. and Luo, J.-L., 2015, "Development of electroless Ni-P/nano-SC composite coatings and investigation on its properties", Surface & Coatings Technology, Vol. 277, pp. 99-106.

Mirza, M.M., Rasu, E. and Desilva, A., 2016, "Surface coatings on steel pipes used in oil and gas industries", American Chemical Science Journal, Vol. 13, pp. 1-23.

Musa, A.Y., Kadhum, A.A.H., Mohamad, A.B., Daud, A.R., Takriff, M.S., Kamarudin, S.K. and Muhamad, N., 2009, "Stability of layer forming for corrosion inhibitor on mild steel surface under hydrodynamic conditions", International Journal of Electrochemical Science, Vol. 4, pp. 707-716.

Palaniappa, M. and Seshadri, S.K., 2007, "Structural and phase transformation behavior of electroless Ni-P and Ni-W-P", Materials Science and Engineering A, Vol. 460-461, pp. 638-644.

Park, S.H. and Lee, D.Y., 1988, "A study on the microstructure and phase transformation of electroless nickel deposits", Journal of Materials Science, Vol. 23, pp. 1643-1654.

Rabizadeh, T., Allahkaram, S.R. and Zarebidaki, A., 2010, "An investigation on effects of heat treatment on corrosion properties of Ni-P electroless nano-coatings", Materials and Design, Vol. 31, pp. 3174-3179.

Szczygiel, B, Turkiewicz, A. and Serafinczuk, J., 2008, Surface morphology and structure of Ni-P, Ni-P-ZrO_2, Ni-W-P, Ni-W-P-ZrO_2, Surface & Coatings Technology, Vol. 202, pp. 1904-1910.

6. RESPONSIBILITY NOTICE

The authors are the only responsible for the printed material included in this paper.